

# Lab on a Chip

Accepted Manuscript



This is an *Accepted Manuscript*, which has been through the Royal Society of Chemistry peer review process and has been accepted for publication.

*Accepted Manuscripts* are published online shortly after acceptance, before technical editing, formatting and proof reading. Using this free service, authors can make their results available to the community, in citable form, before we publish the edited article. We will replace this *Accepted Manuscript* with the edited and formatted *Advance Article* as soon as it is available.

You can find more information about *Accepted Manuscripts* in the [Information for Authors](#).

Please note that technical editing may introduce minor changes to the text and/or graphics, which may alter content. The journal's standard [Terms & Conditions](#) and the [Ethical guidelines](#) still apply. In no event shall the Royal Society of Chemistry be held responsible for any errors or omissions in this *Accepted Manuscript* or any consequences arising from the use of any information it contains.

## ARTICLE

## High Purity Microfluidic Sorting and Analysis of Circulating Tumor Cells: Towards Routine Mutations Detection

Julien Autebert<sup>a†</sup>, Benoit Coudert<sup>a</sup>, Jérôme Champ<sup>a</sup>, Laure Saias<sup>a</sup>, Ezgi Tulukcuoglu Guneri<sup>a</sup>, Ronald Lebofsky<sup>b</sup>, François-Clément Bidard<sup>c</sup>, Jean-Yves Pierga<sup>cd</sup>, Françoise Farace<sup>e</sup>, Stéphanie Descroix<sup>a</sup>, Laurent Malaquin<sup>a</sup> and Jean-Louis Viovy<sup>a\*</sup>

A new generation of the Ephesia cell capture technology optimized for CTCs capture and genetic analysis is presented, characterized in depth and compared with the CellSearch system as a reference. This technology uses magnetic particles bearing tumour-cells specific EpCAM antibodies, self assembled in a regular array in a microfluidic flow cell. 48 000 high aspect-ratio columns are generated using a magnetic field in a high throughput ( $> 3 \text{ ml h}^{-1}$ ) device and act as a sieve to specifically capture the cells of interest through antibody-antigens interactions. Using this device optimized for CTC capture and analysis, we demonstrated the capture of epithelial cells with capture efficiency above 90%, for concentration as low as a few cells per ml. We showed the high specificity of the capture with only 0.26% captured non-epithelial cells for concentrations above 10 million cells per ml. We investigated the capture behavior of cells in the device, and correlated the cells attachment rate to the EpCAM expression on the cell membranes, for six different cell lines. We developed and characterized a two-steps blood processing to allow for rapid processing of 10 ml blood tubes in less than 4 hours, and showed a capture rate of 70% for as low as 25 cells spiked in 10 ml blood tubes, with less than 100 contaminating hematopoietic cells. Using this device and procedure, we validated our system on patient samples with an automated cells immunostaining procedure and a semi-automated cell counting. We captured CTCs in 75% of metastatic prostate cancer patients and 80% of metastatic breast cancer patients and showed similar or better results than the Cellsearch device in 10 out of 13 samples. Finally, we demonstrated the possibility of detecting a cancer-related PIK3CA gene mutation in 20 cells captured in the chip with a good correlation between the cell count and the quantitation value Cq of the post-capture qPCR.

### Introduction

Cancer is the second major cause of death in the industrialized world, in spite of some progress in therapy. The treatment of primary tumors has progressed steadily thanks to chemotherapy, surgery and the development of targeted therapies, but metastases still occur frequently, and are responsible of about 90% of cancer deaths. Circulating tumor cells (CTC) correspond to a critical step of the haematogenous metastatic process and are defined as malignant cells issued from a primary or secondary tumor and escaping in the blood through an intravasation process. From there, they might disseminate into distant organs, (e.g. bone marrow, liver, etc), and initiate new metastasis.<sup>1</sup> Blood being easily sampled and analyzed, CTC are particularly interesting as circulating

metastasis-related biomarkers<sup>2</sup>. Clinically, the number of CTC detected is a strong prognostic marker in both non-metastatic<sup>3</sup> and metastatic breast cancer<sup>4</sup>, as well as in several other tumor types. Moreover, CTC count is used during treatment in metastatic breast cancer patients, as a dynamic biomarker associated with the treatment efficacy<sup>4</sup>. Finally, the molecular characterization of CTC may unravel the biological mechanisms of tumor progression, as well as the presence of key treatment-related biomarkers. For instance, some changes in the HER2 status of breast cancer between the primary tumour and CTCs have been reported<sup>5,6</sup>.

From an analytical point of view, the search of CTCs in blood is a strong challenge<sup>7</sup>. The very low concentration of CTC (about 1 CTC among ten million of white blood cells and billions of red blood cells per milliliter) imposes the need for an

enrichment of the population of interest. As a pioneer, the Cellsearch™ system (Janssen Diagnostics) showed very interesting results regarding the monitoring of metastatic breast, prostate and colon cancer. This approach relies on the extraction of cancer cells from blood using EpCAM-coated (Epithelial Cell Adhesion Molecule) magnetic nanoparticles combined with cells fixation and staining for a visual identification and counting. This system was clinically validated<sup>8</sup> and cleared for clinical use by the American Food and Drug Administration. It however suffers from a moderate inter-laboratory reproducibility (with CV ranging from 45 to 64%)<sup>9</sup>, poor imaging resolution and a number of biomarkers that can be studied simultaneously limited to 4.

The development of new strategies for the capture and analysis of CTCs is continuously evolving, and various innovative techniques were recently proposed. The cell selection criteria can be physical or biological/biochemical.<sup>10,11</sup> In the first case, the selection is based on cancer cell size and/or deformability. These systems are interesting because the cell capture doesn't rely on the presence of any kind of antigen on the cell membrane. However the use of size and deformability of a cancer cells as a selection criterion is still a subject of controversy.<sup>12</sup> In the second case, capture devices use antibodies specifically directed against cancer cell membrane to capture the circulating tumor cells. Obviously, the choice of the capture antibody is critical in such applications. A commonly used capture molecule is the EpCAM antibody, a trans-membrane protein expressed on most normal epithelial cells which functions as a calcium-independent cell adhesion molecule.

Capture using antibodies can be done by flowing the sample to be analyzed on a surface functionalized with the antibody,<sup>13-17</sup> or by mixing and capturing cells with magnetic nanoparticles coated with the antibody (Cellsearch, Magsweeper<sup>18</sup>). The first method requires some time consuming surface treatment, and raises problems of chip-to-chip reproducibility and quality control. The second method has the advantage of being very reproducible (commercial antibodies-coated magnetic beads can be prepared and characterized in large batches), but suffers from some limitations regarding the optical analysis of cells: a large excess of nanoparticles is needed to capture rare cells with a suitable kinetics, and during the magnetic sedimentation process, they tend to lead to a saturation of the cells surface by beads, leading to imaging limitations.

In recent years, however, a new breakthrough seems to have been made in the field of CTC search, associated with the development of microfluidic-based systems. The first publication of the "CTC Chip"<sup>16</sup>, has been followed by the proposition of a number of different microfluidic concepts for CTC search (see Alix-Panabières and Pantel,<sup>19</sup> Autebert et al.<sup>10</sup>, Cima et al.<sup>12</sup> and Chen et al.<sup>20</sup> for reviews).

The Ephesia system,<sup>21</sup> developed for the capture of blood B-cells of leukemia and lymphoma patient, combines the best aspects of microfluidics and immunomagnetic sorting. We present here the latest generation of the Ephesia for CTC capture, and the results obtained both on cell lines and patients

samples regarding cell capture efficiency, post-capture analysis and mutations detection.

## Experimental section

### Microfluidic chip design and fabrication

All experiments were performed in PDMS microchannel devices (Dow Corning Sylgard 184). The fabrication relies on mold casting according to a previously reported soft-lithography procedure.<sup>22,23</sup> Briefly, the master mold was first fabricated by spin-coating SU-8 (2050) negative photoresist (Microchem Corporation) on a silicon wafer that was further exposed to UV light through a photomask film (Selba, Switzerland). Channels were developed with SU8-Developer (Microchem Corporation) and the master mold's surface was treated with Trichlorosilane (ABC R GmbH, AB111444) in order to prevent sticking of the PDMS on the surface. PDMS precursor was prepared with a 10:1 ratio of base and curing agents respectively, poured on the SU8-mold and degassed in a vacuum chamber for ten minutes before curing in a 70°C oven for 4h. The microfluidic chips consists in a two layers stack. The top layer is made of PDMS and comprises the microfluidic channels and the inlet and outlet ports. The bottom layer of the device consists in a microstructured PDMS layer, 50 µm thick, on a 1 mm thick glass backplane. The resulting chip is a 5 mm thick circular PDMS chip (5 cm diameter).

An earlier design of the microfluidic chip was already described and characterized in Saias et al.<sup>22</sup> It was optimized to achieve high flow velocity homogeneity along the capture areas while keeping a very small footprint and a global flow rate around 2 ml h<sup>-1</sup>. Computer simulations (COMSOL) and experimental studies led to an improved design where the branching zone remains smaller than a classic "tree-like" design. The chip used in the present study involves a slightly modified design: inlets/outlets were integrated in the same layer as the capture chambers to facilitate chip fabrication; filtering zones, based on 50 µm spaced PDMS posts, were added at the entrance of the chip in order to prevent debris or dust particles from entering the chamber and causing damages in the columns or channel clogging (see Figure 1.a). The geometry of the distribution channels was also modify in order to accommodate all of them in the same plane and simplify the fabrication process. These changes, however, did not alter the previously characterized flow pattern in the capture areas.

### Magnetic patterning

Magnetic columns must be anchored to the bottom layer of the chip to withstand hydrodynamic flows and remain stable during the whole capture and analysis process. In order to improve the stability of the columns, the previously used contact-printing method<sup>21</sup> was replaced by a capillary assembly technique.<sup>24,25</sup> For this purpose, a microstructured PDMS template with micron sized recessed patterns was fabricated by soft lithography. PDMS was first spin-coated on SU8/silicon mold at 1000 RPM for 30 seconds. After curing, the thin

bottom layer (below 100  $\mu\text{m}$ ) was peeled from the mold and deposited on a clean 5 cm diameter glass slide. The design of this bottom part is made of two capture zones which contains 48000 holes (10  $\mu\text{m}$  deep, 10  $\mu\text{m}$  diameter), arranged in an array (48 rows, 1000 lines). The spacing between holes was set to 60  $\mu\text{m}$  (see Fig 1.a). An aqueous suspension of 2.7  $\mu\text{m}$  carboxylic acid-coated magnetic beads (Dynabeads M-270 Carboxylic Acid 143.05D, Invitrogen Dynal AS, Oslo, Norway) was prepared in a solution of water, Triton X45 (0.1 %), and SDS (0.01 M) with a 2:1:1 ratio. Capillary assembly of particles was performed as described previously.<sup>24,25</sup> The PDMS template was first mounted on a moving translation stage. A defined volume of suspension (10  $\mu\text{L}$ ) was injected between the template and a slide fixed above the substrate at a distance of approximately 500  $\mu\text{m}$ . The template was then translated at a fixed velocity of 30  $\mu\text{m s}^{-1}$ . Experiments were carried out at room temperature. Using this method each hole was filled with five or six particles while no deposition was observed on the flat areas around the patterns.

### Chip sealing and surface treatment

The top layer (comprising the channels) was bonded to the bottom layer (comprising the array of magnetic “anchors”) by treating both PDMS parts using a 200W air plasma (Harrick Plasma, PDC 32G) for 20 s. PTFE tubing (Cole Parmer Corporation) were inserted in the device and a 5% PDMA-AGE in water<sup>26,27</sup> solution, kindly provided by M. Chiari, was injected inside the chip and incubated for 1 hour, under a constant 50 mbar pressure. This surface treatment was used to prevent the non-specific adsorption of beads, cells and proteins. After incubation, the device was washed with PBS (10 minutes at 50  $\mu\text{L min}^{-1}$ ).

### Magnetic columns formation

The microfluidic chip was inserted in a water-cooled electromagnetic coil. The coil consists in 600 turns of 1 mm insulated copper wire. A typical current intensity of 4.5 A was used to generate a uniform 30 mT magnetic field in the center of the microfluidic chip. A suspension containing 25  $10^7$  EpCAM coated magnetic beads (4.5  $\mu\text{m}$  diameter Dynabeads “Epithelial Enrich”) was washed twice with PBS, redispersed in 150  $\mu\text{L}$  of PBS and injected in the chip at a flow rate of 30  $\mu\text{L min}^{-1}$ . The magnetic field was turned on when the first beads were entering the capture chamber. Injection was maintained during 3 minutes in order to supply enough particles to create columns over the whole capture area by magnetic assembly. Beads in excess were washed away with PBS at 50  $\mu\text{L min}^{-1}$  during 5 minutes and could be recovered.

### Liquids handling and automation

All the samples used during the experiment were stored in pressurized containers directly connected to the microfluidic chip. An MFCS-8C Flow Controller (Fluigent, France) was used to control the pressure independently in each container. An additional module, Flowell (Fluigent), was used to monitor

and control the global flow rate at the outlet of the chip. In addition, two computer controlled rotatory valves with a 50  $\mu\text{L}$  internal dead volume (Fluigent) were used in order to inject the sample and reagents in the chip. Automation of the sample injection sequences (surface treatment, beads suspension, sample, rinsing solutions, and fixation and labeling agents) and flow rate regulation was performed using the Maesflow software (Fluigent).

### Cell lines culture and sample preparation

Cell culture reagents were purchased from Gibco (Gibco, Grand Island, NY). MCF7, SKBR3, MDA-MB-231, PC3 and A549 epithelial cell lines from ATCC were used for the spiking experiments. Those cell lines were cultured in DMEM-GlutaMax supplemented with 100  $\text{U ml}^{-1}$  aqueous penicillin, 100  $\text{mg ml}^{-1}$  streptomycin and 10% foetal bovine serum (FBS) at 37°C in a humidified atmosphere with 5%  $\text{CO}_2$ . Cells were harvested using 0.05% Trypsin/EDTA. Lymphoid cell lines used for the control experiments are RAJI (B lymphocytes derived from a Burkitt's lymphoma) cell line from ATCC. They were cultured in RPMI 1640 medium-GlutaMax supplemented with 100  $\text{U ml}^{-1}$  aqueous penicillin, 100  $\text{mg ml}^{-1}$  streptomycin and 10% foetal bovine serum at 37°C in a humidified atmosphere with 5%  $\text{CO}_2$ . After harvesting cells, the resulting cell suspension titre was determined using a hemocytometer (Malassez chamber) and diluted to obtain the desired cells concentration. For very low cell concentrations, multiple counts were done using the same counting method to reduce fluctuations.

Blood pre-treatment was achieved by Ficoll-based gradient density centrifugation. Briefly, EDTA blood samples were layered on top of Ficoll-Paque PLUS (GE Healthcare, Uppsala, Sweden) and centrifuged at 400g for 30 minutes at 20°C. In the case of Cellsave tubes, blood samples were submitted to a CD45 positive cell depletion (RosetteSep™ Human CD45 Depletion Cocktail (StemCell Technologies Inc., Vancouver, BC, Canada) before the gradient density centrifugation.

Processes for blood preparation were defined as follow: i) blood samples below one ml were processed raw, after a three time dilution. ii) fresh blood samples (no fixative, 7.5 ml EDTA tubes) were centrifuged once to remove the RBC, and processed. iii) Fixed blood samples (CellSave tube, Janssen Diagnostics) would be incubated with the Tetrameric Antibodies Complexes and centrifugated to remove RBC and most of the CD45 expressing cells.

All patient samples were collected after written informed consent. Metastatic prostate cancer patients have been included in the Gustave Roussy promoted study CEC-CTC (CSET 2008/1370, 2008-A00585-50). Metastatic breast cancer patients have been included in an Institut Curie-promoted study (NCT02220556).

### Fluorescent staining

Hoechst nucleus staining (Hoechst 33342, Invitrogen) was used for rapid counting and visualization of a single cell line

population. For that purpose, 150  $\mu\text{L}$  of a 5  $\mu\text{g ml}^{-1}$  solution of Hoechst diluted in PBS was flown inside the chip for 10 minutes and incubated into the capture zone for 20 more minutes. Rinsing was then achieved by flushing 150  $\mu\text{L}$  of PBS at a 30  $\mu\text{L min}^{-1}$  flow rate.

For more complex cell mixtures (such as few MCF7 epithelial cells mixed with millions of RAJI cells and clinical samples), cell discrimination was achieved through multiple fluorescent immunostainings: an epithelial cell was defined as a cell with a diameter above 6  $\mu\text{m}$ , a nucleus, a positive Cytokeratin (CK) staining and no CD45 staining. Antibodies were purchased from Dako (Glostrup, Denmark). Pan-Cytokeratin antibody (clone AE1/AE3) was used as a target for intra-cellular positive stainings and CD45 (clone 2B11 + PD7/26) antigens as a target for membrane negative staining. Prostate cancer cells were stained for PSA antigen (clone ER-PR8). Fluorescently labelled secondary antibodies were purchased from Invitrogen (Alexa Fluor 488, 555 and 647). The protocol consisted of nucleus staining with Hoechst (30 minutes, 5  $\mu\text{g ml}^{-1}$ ), rinsing (5 minutes, 30  $\mu\text{L min}^{-1}$ ), membrane staining (30 minutes, 1  $\mu\text{g anti-CD45}$  antibodies with 5  $\mu\text{L AF488}$ ), fixation (Invitrogen Fix & Perm Reagent A, 15 minutes) and finally Cytokeratin staining (1  $\mu\text{g anti-CK}$  antibodies with 5  $\mu\text{L AF555}$  + Invitrogen Fix & Perm Reagent B, 20 minutes).

### Imaging platform and cell counting

Images of the immobilized and stained cells were acquired using a Nikon TI-E inverted microscope equipped with a motorized x/y stage, automated z-focus and a Photometrics CoolSNAP HQ2 camera. Counting of the cells was done with a first automated nucleus detection and a manual counting of all Cytokeratin+/CD45- cells. Details on the imaging procedure and cell counting can be found in Supplementary Information (S.I.).

### Mutation detection

After capture and visualization, bead-cell complexes were released and collected by switching off the magnetic field and flushing the Ephesia chip with PBS. Cell lysis was then performed by resuspending the sample in a freshly prepared 50 mM NaOH solution followed by an incubation step (95°C for 30min). Finally, a 50mM TrisHCl (pH 8) solution (equal volume of NaOH) was added to neutralize the solution used in the lysis step. Beads were removed using a magnetic separator stand and the supernatant was used for qPCR.

Forward and Reverse primers and TaqMan probes (wildtype and mutant) designed to target the PIK3CA mutations c.1633G>A/E545K were kindly provided by the Circulating Biomarker laboratory at the Institut Curie.

Real-time PCR was carried out in a 25  $\mu\text{L}$  reaction mixture containing 1X TaqMan Universal PCR Master Mix (Life Technologies), 400nM of each Forward and Reverse primers, 200 nM probe (wildtype or mutant), and 5  $\mu\text{L}$  of DNA template. Thermal cycling was performed on a SmartCycler

(Cepheid) system with the following conditions: 95°C for 10 min and 50 cycles of 95°C for 15 s, 60°C for 1 min.

## Results and discussion

### Immunocapture of rare cells using the Ephesia technology

The Ephesia technology,<sup>21</sup> previously developed for the capture of white blood cells, had to undergo numerous modification and improvements to tackle the complex problem of rare cells sorting from blood, and to lead the device to a validation on clinical samples. The core of the microsystem involves the self-assembly, in a microchannel, of a regular array of capture columns made of antibodies-coated magnetic beads directed against CTCs. This technology relies on the capability of superparamagnetic beads under a magnetic field to self-assemble into a periodic array of high aspect ratio columns, with a spacing defined by the magnetic template at the bottom of the cell. Those columns, assembled perpendicular to the flow, create a dense sieve and cells flown through will collide multiple times with the beads. By coating those beads with the desired antibody, cells presenting the antigen of interest on their membrane can be captured while the remaining cells are taken away by the flow. This technology avoids the need of costly and complex microfabrication processes. Another advantage of this method is the possibility of creating very high aspect ratio (above 1:10) antibody-coated columns at will, and to flush them away (by removing the magnetic field) if needed. Interestingly, the total available surface for capture and the flow rate increase with the aspect ratio of the columns, at equal footprint of the device and flow velocity.

Because CTCs are scarce (a few CTC in a 10 ml tube of blood), the Ephesia device had to be optimized to provide a flow rate compatible with the processing of large volumes. An optimized microfluidic geometry, called “diamond-like shape” was previously developed<sup>22</sup> to ensure a homogeneous flow velocity and uniform spreading of the cells in the capture areas containing an array of 48 000 columns. The global footprint of the device was restricted to 5 cm in order to limit the size of the magnetic coil required to maintain the columns stability. With this design, the columns assembled from 4.7  $\mu\text{m}$  beads could sustain without damage flow velocities up to 1  $\text{mm s}^{-1}$  for a 50  $\mu\text{m}$  deep channel, corresponding to an operating flow rate of 3  $\text{ml h}^{-1}$ . Additionally, the use of a capillary assembly method<sup>28</sup> to create the magnetic anchors showed to be more reliable than the previously used patterning method, leading to a drastic increase of the column resistance to flow.

### Investigating cell capture mechanisms and efficiency

A strong advantage provided by immunocapture is the very high specificity of the antibody/antigen interaction. We choose the anti-EpCAM antibody for every validation step as this antibody has been proven to be clinically relevant, and is used in routine in the Cellsearch device, thus avoiding to the best extent biomarker bias in comparisons with this established technology.

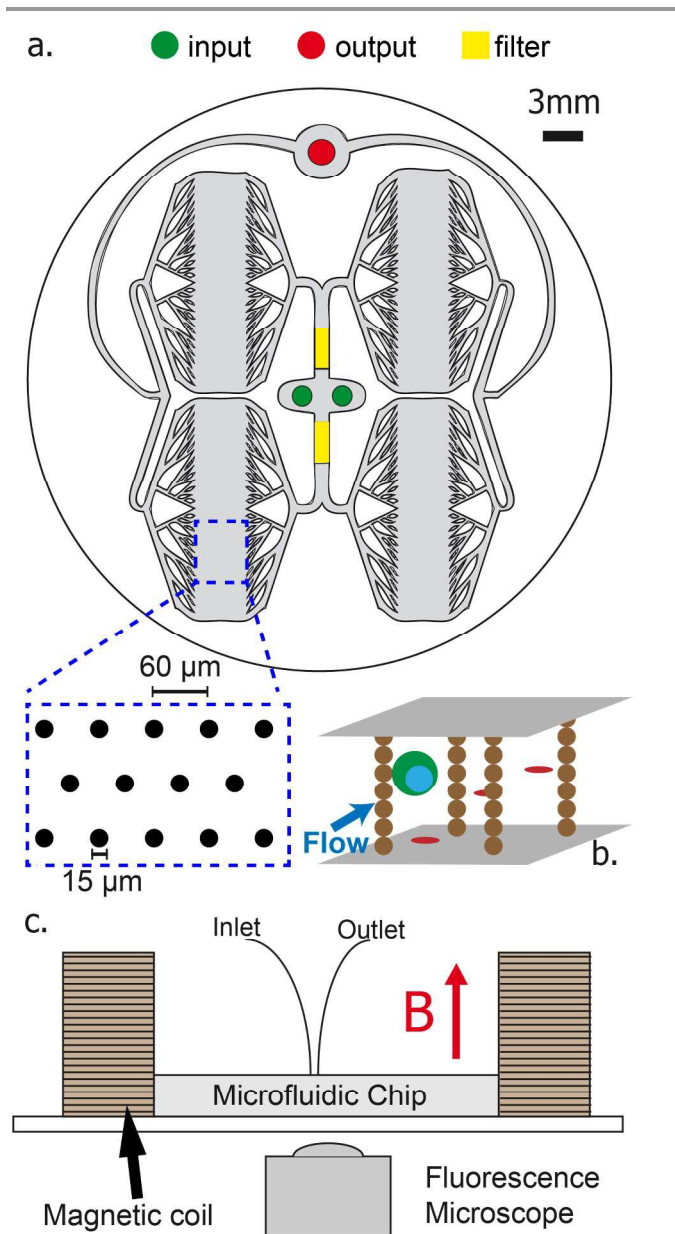


**Figure 1.** Description of the Ephesia device, modified for CTC capture. **a.** Sample is flown through a diamond-like chip to the capture zones where an hexagonal array of columns are lying. Spacing between adjacent columns is  $60\ \mu\text{m}$  and anchors are  $15\ \mu\text{m}$  in diameter. **b.** Scheme of the cells flowing through the columns array. Epithelial cells (green) are captured on the columns while leucocytes and red blood cells (red) flow through. **c.** Chip is placed inside a magnetic coil on top of an inverted fluorescence microscope. The magnetic field ( $30\text{mT}$ ) required to form the columns is oriented upward.

Targeting this specific membrane protein, we first investigated the capture capacities of the device on EpCAM-positive and EpCAM-negative cell lines. It is important to notice that our method is easily adaptable to any type of commercially available or home-made antibody-coated beads library.

When a cell enters the capture area, the interaction between the antibody on the bead surface and the antigen on the cell membrane is possible if a collision occurs between the bead and the cell. Upon contact, a specific antibody-antigen interaction will bind the cell of interest to the beads, while unwanted blood cells are washed away by the flow. The efficiency of the capture therefore depends on the probability of collisions between beads and cells, and thus on the distribution of flow within the column array. To promote these interactions, the gap between columns as well as the pattern of the columns array has been optimized according to the size of the cells of interest. Among different designs (results not shown), we demonstrated that a hexagonal array (see Figure 1.a) with a spacing of  $60\ \mu\text{m}$  is suitable for the sorting of cells with a diameter ranging from  $10$  to  $30\ \mu\text{m}$ . Kirby's group<sup>29</sup> showed that a shift in the position of the columns could increase the probability of contact. In the case of the Ephesia device, we did not observe a significant improvement of the capture by shifting columns every row. Indeed, contrary to regular silicon/PDMS columns, Ephesia columns are mostly arranged as a linear array of single to few spherical beads. This high aspect ratio considerably reduces the deviation of low lines and the subsequent "wake" of one column. In addition, they are not perfect, and defects such as the random presence of additional beads on the side of columns probably adds to the flow pattern a local random component that further reduces the range of the "wake effect" discussed in<sup>18</sup>, increasing the probability of contact between cells and columns.

Other parameters involved in the capture efficiency are i) the surface density of antibodies on the beads, ii) the thermodynamic affinity constant between the antibody and the antigen in the capture buffer, iii) the duration of the contact, iv) the hydrodynamic force exerted during contact, and v) the antigen expression levels on the cell membrane. Both the antibodies density on the magnetic bead surface (i) and affinity (ii) were fixed by the commercial beads we used (Dynabeads® Epithelial Enrich), grafted with the mouse IgG1 monoclonal anti-EpCAM antibody (clone Ber-EP4). The affinity and selectivity of this antibody was found to be similar to mAb clones HEA125 used in the vast majority of anti-EpCAM capture methods. The potential influence of the contact duration (iii) and strength (iv) was evaluated by varying the flow velocity in the capture area. No significant differences were observed in the range of flow rate investigated (from  $0.5\ \text{ml h}^{-1}$  up to  $3\ \text{ml h}^{-1}$ , i.e.  $1\ \text{mm s}^{-1}$ , results not shown). Flow velocities above  $1\ \text{mm s}^{-1}$  could not be investigated, as the columns do not withstand the resulting hydrodynamic drag. As a consequence, we believe that in these conditions, the antigen-antibody interaction kinetics is not limiting the capture efficiency. Finally, the antigen expression level on the cell membrane (v) was investigated extensively (see paragraph below/see "Antigen expression and capture profile" section).

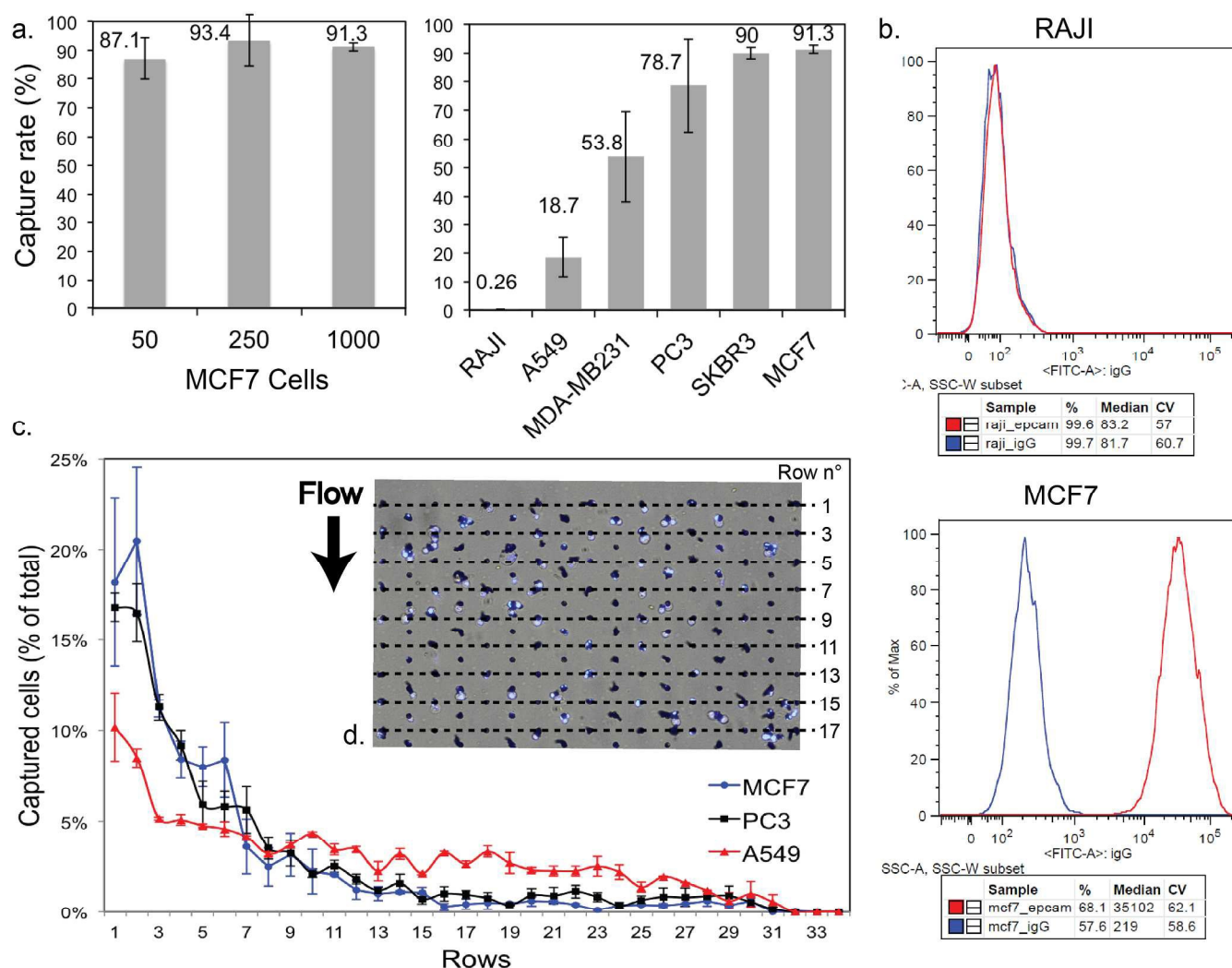


**Figure 2.** a. Capture rates for different quantity of MCF7 epithelial cells: 50 (N=4), 250 (N=4) and 1000 (N=4) cells, and for different cell populations (RAJI, A549, MDA-MB231, PC3, SKBR3 and MCF7) b. Flow-cytometry was used to measure EpCAM expression for two cell lines (RAJI and MCF7). EpCAM (red) and isotype control (igG, blue) are presented with median value and standard deviation. (For others cell lines, see S.I.) c. Capture profile obtained for 3 different cell lines. The percentage of capture cells was defined as the ratio of the number of captured cells for each row to the total number of captured cells. For more convenience, only the first 34 rows (out of 48) are presented. d. Optical images of the columns array after the capture of MCF7 cells. The cells (nucleus in blue) are captured on each rows of the device. Rows are counted from top to bottom, in the direction of the flow, to obtain the capture profile.

As a first validation step, we processed small sample volumes (between 300  $\mu$ L and 500  $\mu$ L) containing variable quantities of EpCAM-positive cells (MCF7 cell line), spiked into PBS and used as a CTC model. The percentage of captured cells was defined as the ratio of cells counted on the columns to the cells spiked in the sample. Figure 2.a shows the results obtained for three different initial numbers  $N_0$  of spiked cells at averages ranging from 50  $\pm$  3 to 1000  $\pm$  10 into 300 to 500  $\mu$ L of sample. All the experiments showed a similar capture yield with an average of 90.6%  $\pm$  5.84% (n=12) captured cells. To the best of our knowledge, this capture efficiency is amongst the highest obtained using microfluidic devices. We expect that the large available area of capture, the small diameter of the columns, increasing the “head-on” character of collisions, and the randomness of flow paths through the chip are responsible for this excellent capture rate value. Cell loss occurring out of the chip (and therefore not accountable by means of

fluorescence microscopy) may be due to non-specific adsorption on connecting tubes and reservoir. In these experiments the cells concentration was not a limiting factor, as the maximum capture capacity of the device was not reached. To investigate this maximum capacity, we performed experiments with higher concentration of MCF7 cells. An identical capture rate of above 90% was measured for samples containing 5000 cells or more (results not shown). We envision the maximal number of captured cells to be above  $10^5$  (two cells captured on each of the 48000 columns).

The non-specific capture rate is defined as the proportion of EpCAM-negative cells captured on the columns after spiking a large excess of those cells. To estimate this rate, we first drove high concentration ( $10^7$  cells per ml) EpCAM-negative lymphoid cells (RAJI cell line) inside the chip at the standard flow rate. Nucleus counting using fluorescence microscopy showed that for an initial value of  $10^6$  cells entering the chip,

only 0.26% +/- 0.13% (n=3) of the cells were non-specifically captured on the columns (see Fig 2.a, RAJI cell line). As previously observed, no significant influence of the flow rate on the non-specific capture was observed in the range of flow rates investigated.

Finally, we measured both the efficiency and specificity of the capture on mixed population of cells (MCF7 and RAJI) in order to mimic blood samples composition. Both specific and non-specific capture efficiencies were investigated with cells suspensions containing 50 EpCAM-positive cells and  $5.10^6$  EpCAM-negative cells in 500  $\mu$ L of PBS. The results showed that the Ephesia device provides an efficient and selective enrichment of the EpCAM-positive population: an average of 90% +/- 1.4% (n=3) EpCAM-positive cells were recovered while only 0.2% +/- 0.11% (n=3) EpCAM-negative cells were non-specifically captured. These results are consistent with the high capture efficiency observed, and show that the overwhelming excess of EpCAM-negative cells does not deteriorate the capture through screening of the cells of interest, nor increase the rate of non-specific capture.

### Antigen expression and capture profile

MCF7 cells have a moderate to high expression level of EpCAM protein on their membrane. However, in real samples, this expression level can vary, especially if the CTC is undergoing an epithelio-mesenchymal transition. One of the most commonly used arguments against EpCAM-based cell sorting devices is that numerous cells might be lost when expression decreases. To investigate the role of EpCAM expression on the capture, we used four cell lines (SKBR3, PC3, MDA-MB-231 and A549) that showed lower expression levels of EpCAM (as compared to MCF7 taken as a reference) when measured using a flow cytometer (Fig 2.b). For each cell line, both EpCAM (red) and isotype control (IgG, blue) are presented with median value and standard deviation (see Fig 2.b). for RAJI and MCF7, and other cell lines results are given in S.I. (S2). Knowing the expression level, we investigated the capture rate of the SKBR3, PC3, MDA-MB-231 and A549 cell lines by standard spiking experiments. Capture rates are presented in Figure 2.a. The results show that, as expected, the capture rate was reduced when using low EpCAM expressing cells. The capture rate was 90 +/- 2.0 % (n=4) For SKBR3 (medium expression) 78.7 +/- 7.2 % (n=4) for PC3 (low expression), and 18.7 +/- 6.8% (n=4) for A549 (very low expression). For EpCAM-negative RAJI, the capture rate was 0.26 +/- 0.13% (n=3). These results are contradictory with some other EpCAM-based capture devices where different levels of EpCAM gave identical capture rate, but similar to recent results obtained with anti-HER2 antibodies<sup>17</sup>. In published work investigating low-expression cells using the Cellsearch device, results showed capture rates around 30% for the MDA-MB-231 cell line which has low EpCAM expression (12 000 antigens per cell) and less than 2% for T24 cell line, which has a very low expression (2100 antigens per cell)<sup>30</sup>. In comparison, we measured a capture rate of 53.8% +/- 15.7% (n=4) for the

MDA-MB-231 cell. For each cell line, the capture rate in our system remains above the one obtained with the CellSearch device, even for low EpCAM expression.

An interesting way of investigating the capture process in detail is to count the number of cells captured for each of the 48 rows of the Ephesia chip. This “capture profile” (see Figure 2.d insert – MCF7 cell line) has been previously described<sup>21</sup> for large quantities of captured cells, where columns can become saturated. In the Ephesia CTC device however, saturation has little chance to occur and the capture profile can be described by the following simplified model: each cell entering the array of columns has a probability  $\beta$  of colliding with a column and get captured. This probability remains the same across the whole device. Intuitively, if a cell has a high EpCAM expression (and therefore a high  $\beta$ ), it will more likely get captured in the first few rows, leading to a capture profile defined by a rapid decrease of cell count upon “depth” in the array. Oppositely, a low-expressing cell will have a relatively flat profile, with a lower capture rate per row (and a lower  $\beta$ ) but a larger depth of penetration. Figure 2.c shows the capture profiles obtained for three cell lines with varying EpCAM expression. As expected, high to low expression cells (MCF7, PC3) are mainly captured in the first few rows and the capture count decreases rapidly while the A549 cell line has a flatter profile, consistent with its very low EpCAM expression. Interestingly, we did not observe any A549 cells captured after the 31<sup>st</sup> row while we were expecting a flat profile. We propose the following tentative explanation for this discrepancy: i) after capture, there is a balance of forces between adhesion forces of the antibodies/antigens interactions and the shear force of the flow. Thus a minimal amount of interactions between the cell and the bead is required to promote an irreversible capture for a given flow rate. For all cells lines, flow cytometry showed that there is an important polydispersity regarding EpCAM expression. Thus for such low expression cells as A549, we can assume that a vast majority of the cells (around 80%) presents an antigen count too low to be captured by the Ephesia chip, but cells with an expression suitable to be captured have made at row 31 enough collisions to be almost certainly captured.

Globally, these results enlighten the high quality of capture for all type of cells considered as EpCAM positive, and show that even cells with a very low EpCAM expression can be captured with a decent efficiency, while EpCAM negative cells are not contaminating the capture zone.

### Optimizing blood sample processing

The results obtained on model samples show the excellent capture efficiency and purity provided by the Ephesia device. However, recovering CTC from patient’s blood samples is a more challenging and delicate operation, due to the complexity of the sample to be analyzed. Additional difficulties are associated with blood, notably viscosity, possible screening of collisions by red blood cells (RBC), and sample conservation. Because of blood viscosity, samples cannot be processed

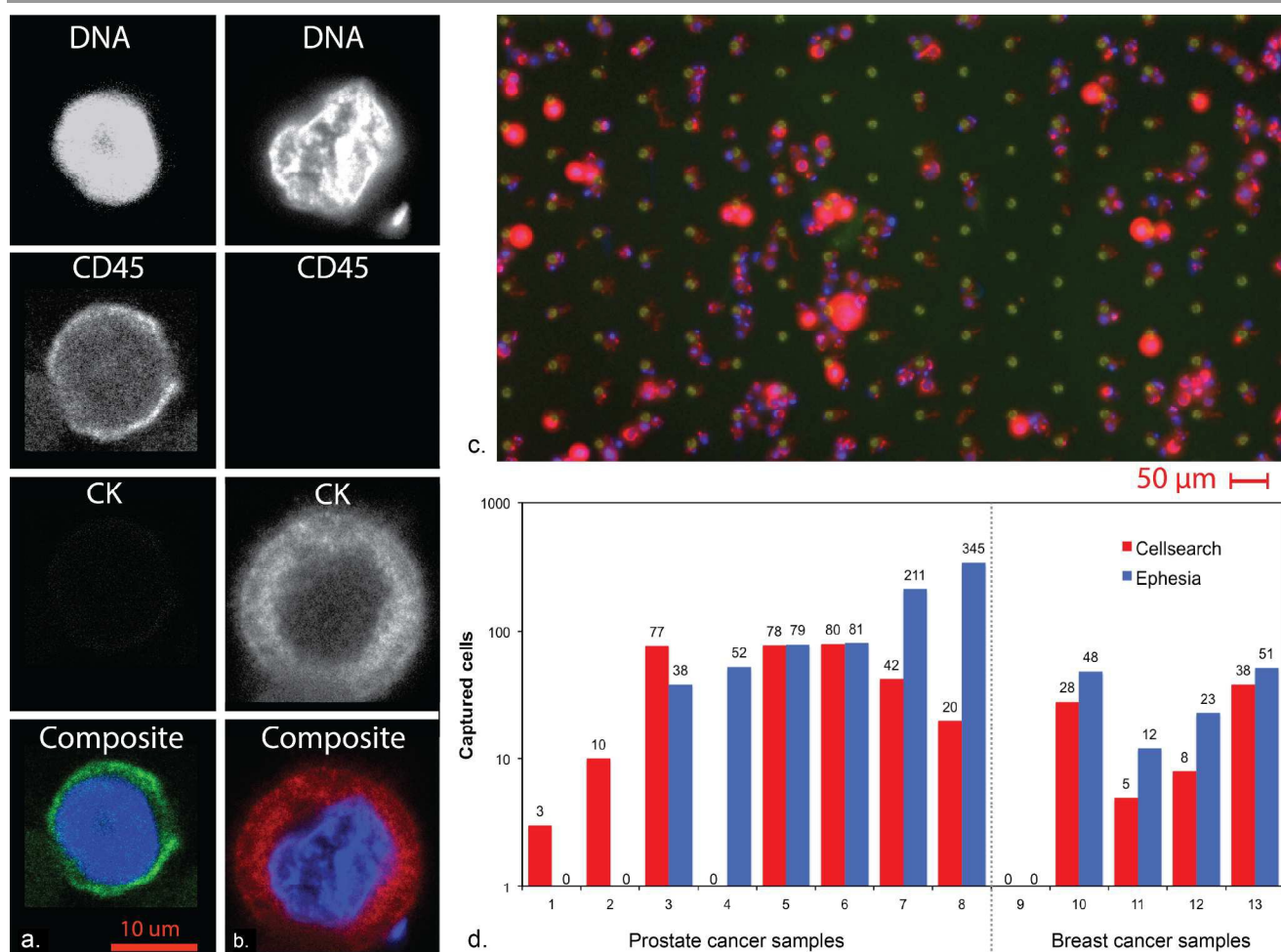


**Figure 3.** CTCs observation and counting. **a & b.** Cell characterization is performed through Nucleus, CD45 and Cytokeratin (CK) stainings that allow to distinguish leucocytes (**a**) from epithelial cells (**b**). **c.** Cancer cells captured from a lumbar puncture of a neoplastic meningitis derived from a breast cancer patient. Nucleus is stained in blue and Cytokeratin in red. Beads dim fluorescence (green) shows the array of columns. **d.** CTC counts obtained from 8 metastatic prostate cancer patients and 5 metastatic breast cancer patient using the Ephesia device. Each sample was analyzed and compared to the Cellsearch gold-standard method. The dotted line shows the separation between the two sample origins (breast and prostate cancers).

directly in the Ephesia chip at flow rates sufficient for treating milliliters of samples, since the shear forces would destroy the columns. Additionally, RBC might have a screening effect on the cells of interest, and tend to reduce capture efficiency. To overcome this problem, different approaches were investigated to remove RBC from blood.

Lysis of the erythrocytes showed to be incompatible with our device: lysis processes involving a fixation step dramatically increased the non-specific capture of white blood cells, while fixative-free lysis reduced the capture rate by damaging the cells' membrane. Gradient-based centrifugation methods appeared as more promising regarding the preservation of the cell membrane. In addition, such method offers a reduction of the volume to process so that the purified extract from a 10 ml sample could be flown in less than one hour. Although the centrifugation steps reduce the global yield (when compared to raw blood), we obtained a capture yield of 69.5% (+/- 7%) for 25 (N=2) and 100 (N=2) cells in average (following a Poisson distribution) spiked in 10 ml blood collected in EDTA tubes from healthy donors and spiked with

MCF7. Although lower than for cells spiked in buffer, this capture yield remains high compared to the literature and is suitable for clinical work. Negative controls (healthy donors blood, no cells spiked) showed to be repeatedly negative (N=10, results not shown) with no Cytokeratin positive/CD45 negative cells counted in any of them.

Using the device in a clinical context requires careful investigation of the stability of the samples over time prior to their processing. To this end, we investigated the possibility of transporting (overnight shipment through Europe) and storing blood samples for several days (up to 72 hours) prior to analysis. Cellsave sample tubes (Janssen Diagnostics) containing a fixative and spiked with unknown amount of cells (ranging from 10 to 100 cells) were sent from Germany. By comparing the results obtained on those samples with the Cellsearch gold-standard method, we showed a concordance of the Ephesia count against the Cellsearch count of 87.4% (+/- 39.4%) (N=5, results not shown), unveiling the ability of the Ephesia device to capture efficiently cells from blood samples in long-conservation conditions. However, for fresh samples,

we observed a dramatic increase in non-specific adhesion of white blood cells (WBC) when using fixative inside the collection tube (such as in Celsave tube), especially after 48 hours. To overcome this problem, for the samples collected on Celsave tubes, we proposed to combine the Ephesia Capture with “RosetteSep”, an adapted method in which a tetrameric antibody complex recognizing CD45 and glycophorin A was added during the centrifugation process to cross-capture RBCs and WBC. This step showed an improvement of the specificity while reducing further the volume to process (3 ml down to 1 ml). Furthermore, we did not measure any statistically relevant decrease of the capture efficiency while using the RosetteSep protocol.

We therefore showed that the new generation of Ephesia chip that has been optimized for CTC capture, was able to capture CTC from large (>7.5 ml) blood volumes containing low count (below 10 cells) of spiked cells with a high efficiency and selectivity and thus is suitable for clinical applications.

#### Validation on clinical samples: Capture of CTCs from patient

Experiments were carried out on samples from metastatic cancer patients. The samples were collected, transported and processed the same day using the previously described protocol. To compare our device to the gold-standard method (the CellSearch device), we used the classical definition of a CTC admitted by the community, namely: CTC have a nucleus (Hoechst staining), are CD45 negative and Cytokeratin positive. By using fluorescently-labeled CD45 and pan-Cytokeratin antibodies, cells of interest were imaged using a 100x to 400x magnification on an inverted microscope, inside the chip (see Figure 3.a and 3b). The threshold for Cytokeratin positivity was defined as a signal intensity higher than the mean signal coming from the very low autofluorescence of the magnetic beads in the Cy3 channel.

As a first run-in experiment on patient samples, we analyzed in the chip a few tens of microliters of a cerebrospinal fluid from a metastatic breast cancer patient diagnosed with meningeal carcinomatosis. Although this type of sample is relatively rare and thus of limited interest clinically, such samples are interesting models for method characterization: they contain the full substrate complexity of a real patient sample, and cells from patients that are also more representative of the complexity of real clinical situations than spiked cell lines. As compared to CTC, however, they generally contain many more cancer cells than blood, and thus provide better statistics for developing and assess post-capture characterization protocols. We observed the capture of numerous epithelial cells on the columns (see Figure 3.c). The cerebrospinal fluid was processed without any pre-treatment, and was used as a model of patient-derived sample with low leukocyte and red cell content to validate the staining antibodies. In this image, cells were captured mainly in the first rows (only 18 rows out of 48 are visible). Upon capture, the shear forces on the cell-bead complex promoted the rotation of the column, so that the cell was dragged at the rear part of the

column relative to the flow, minimizing the shear force. This rotation of the column is an additional advantage of the method, since the column will present a cell-free surface for the next incoming cell to adhere to. Finally, we can see in the example the variety of staining intensities (Cytokeratin expression, red) and a significant heterogeneity in tumor cell size that typically characterizes real CTCs as compared to cell lines.

To confirm the efficiency of the Ephesia technique for the capture of CTC from patients' samples, we processed blood from metastatic breast cancer (n=5) and metastatic prostate cancer (n=8) patients, and compared our results with the results obtained with the Cellsearch technique on the same patient sample (see Figure 3.d). Four tubes of the same volume were collected from consenting patients, out of which one was processed in the Ephesia chip, and one in the Cellsearch device in parallel. Scoring was performed independently and in a blind process. CTCs were detected in 6 of 8 prostate cancer patients (75%, mean = 119 CTCs per blood tube) and in 4 of 5 breast cancer patients (80%, mean = 27 CTCs). In 10 out of 13 samples, the Ephesia method showed similar or higher quantities of captured cells than the Cellsearch device. Interestingly, in cases where the cytokeratin signal intensity was ambiguous (samples 7 and 8, Figure 3.d), an additional staining of the Prostate Specific Antigen in the far-red spectrum (Cy5) was performed, providing a more precise counting of the CTC. These experiments unveiled cells that did not express high level of cytokeratin and, therefore, that might have been considered as negative events in the Cellsearch device. This observation confirms that the versatility of the Ephesia device, and the ability to adapt staining as a function of the cells of interest is a powerful tool for CTC observation and counting. Overall, out of 13 samples, one was scored negative by both methods, one positive by Ephesia only, two positive by CellSearch only, and nine positive by both methods. In addition, thanks to the periodic positioning of the capture elements, to their high aspect ratio and small footprint along the optical path, and to our dedicated software, the method is prone to a fully automated image analysis and scoring, in contrast with the Cellsearch protocol, which implies an operator-based scoring. Finally, because the columns are oriented along the optical path of imaging, cell imaging is not perturbed by the beads.

#### In-situ analysis and mutations detection

While CTCs are currently used for patient follow-up and prognosis in a “counting” mode, genotyping could be of tremendous interest in a clinical context to unveil the apparition of potential mutations leading to drugs resistance or to inform for targeted therapy eligibility. Moreover, understanding the change in the genotype of CTC during the course of the metastatic evolution could improve the understanding of the disease mechanism.

As we previously mentioned, using the pretreatment of blood based on an antibody-enhanced gradient density separation method, we observed a significant decrease of the non-specific capture of unwanted white blood cells, as

compared to Cellsearch capture or standard centrifugation methods. The very high purity level obtained using the Ephesia system (below 100 contaminating cells in a 7.5 ml blood sample) could potentially provide a powerful platform for further genotype analysis of the captured CTC.

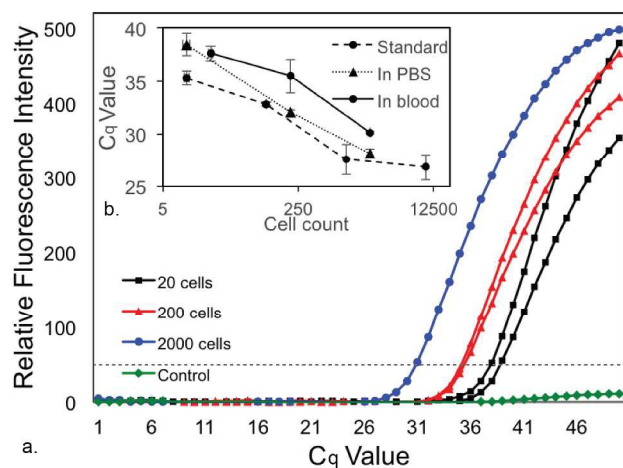


**Figure 4.** qPCR experiment were performed to detect the PIK3CA c.1633G>A/E545K mutation starting from 0 (N=3), 20 (N=2), 200 (N=2) and 2000 (N=2) MCF7 cells, after spiking in PBS and capture inside the Ephesia chip. **a.** qPCR curves (Cq) obtained for different MCF7 cell counts and negative control. **b (inset).** Cq values obtained for standard curve (MCF7 cells not flow through the chip), MCF7 cells spiked in PBS and blood.

As a first validation, we investigated the detection of gene mutations in cells after capture in the chip. We focused on the PIK3CA gene. Cancer-specific mutations have been identified in this gene, causing deregulation of the PIK3 pathway<sup>31</sup>. PIK3CA is mutated in a broad range of tumor types, including uterus (53%), breast (32%), head and neck (21%) and colorectal (15%) cancers. We particularly aimed for the amino acid substitutions E545K located in a hot spot mutation zone.<sup>32</sup> We selected this mutation for its potential use for prognostic, predictive response to treatment and information regarding drug resistance.

MCF7 cells possess 4 copies of the chromosome 3 and are heterozygous for the E545K mutation on exon 9 of PIK3CA gene. Different concentrations of MCF7 cells (from 10 to 2000 per ml) were resuspended in PBS and processed through the chip. After nucleus staining and counting, the whole chip was flushed with PBS. Cells and beads were then collected for analysis by removing the magnetic field. DNA extraction was achieved off-chip and conventional quantitative PCR of the mutation of interest was performed. Results presented in figure 4.a. demonstrates the possibility of detecting the mutation for 13 cells captured (Cq : 37), 130 cells (counts: 128 and 141, Cq: 34.4 and 34.6) and 1000 cells (counts: 1250 and 1000, Cq=30.2 and 30.1), while no signal was observed in negative controls (n=3) and wild-type cells. Finally, we processed similarly six blood samples from healthy volunteers, spiked with different cell counts and observed an increase of the Cq value by 0.5, possibly due to the presence of contaminating cells. Figure 4.b. shows the evolution of the Cq value as a function of cell count for cells not flow through the chip (standard calibration curve

performed in tube), for cells spiked in PBS and cells spiked in blood and captured on the Ephesia chip. We conclude that the Ephesia chip is suitable for the post-capture analysis of as few as 13 cells. However, we are confident that an optimization of the cell recovery and the qPCR protocol will lead to the possibility of detecting even lower amount of cells.

These results are consistent with the ability of the Ephesia device to extract molecular material from captured CTC with low non-CTC contamination levels that allow detection and genetic characterization by conventional PCR methods, of clinically relevant quantities of CTC in blood samples.

## Conclusions

The Ephesia technology, combining magnetic immunocapture and microfluidics, was applied to the capture of cancer cells from model samples involving cell lines with different levels of expression of EPCAM, and from clinical samples, and compared to results achieved with the CellSearch system on the same samples. Promising results for the capture of rare cells from blood were obtained, with yield comparable to or better than current state of the art methods, and a very low level of contamination by non-cancerous cells. Capture of CTCs from patient samples, and comparison to the FDA approved standard method showed the efficiency of the Ephesia device in clinically relevant situations. Moreover, a major interest of this technology relies in its versatility, in particular for the choice of the target antibodies. Indeed, if the EpCAM antigen was chosen as a target, due to its extended use in research, the device is adaptable to any type of antibody, by simply changing the type of beads used. In addition, one can foresee the use of multiple antibodies in a single chip to promote higher capture efficiency, or to perform differential analysis of the expression of different antigens.

We showed that standard centrifugation based methods (a step also present in the Cellsearch device) allows the processing of 10 ml of blood in less than a few hours, while increasing drastically the purity of the complete process.

The Ephesia system also shows promise as a companion for the development and generalization of targeted therapy and high content diagnosis, in which CTC counting will not be sufficient. We demonstrated the potential use of the microfluidic chip to perform further characterization of the captured cells, by means of immunostainings but also through genotyping of the cells. Detection of a specific mutation even from very low number of cells (typically 10 cells in a 10 ml blood volume) was successfully achieved, due to the high purity of the remaining sample after the complete process. This high purity could also be the basis for even more challenging genotyping, such as whole genome sequencing.

From a clinical perspective, the Ephesia device is compact, and can be fully automated, including chip preparation, sample injection, staining and image analysis and scoring, and purified sample retrieval for further genetic analysis. It thus has the potential for non-invasive monitoring of the disease progression, along with detection of targets for innovative

therapies, and drug-resistance mutations detection, thus adding a valuable tool to the oncologist's arsenal.

## Acknowledgements

We thank Cecile Bureau for her support in sample processing and Jordan Madic for his support in the development of the qPCR protocol. We thank Remy Fert and Benoit Lemaire from the UMR 168 workshop for their continuous support. The authors thank Fanny Billiot for expert technical assistance. We are grateful to the Laboratory of Tumor Immunology and the Department of Gynecology and Obstetrics from the University Hospital Munich (Ludwig-Maximilians-University) for sending spiked samples abroad. This work was supported in part by the EU projects CAMINEMS (NMP F7) and "DIATOOLS (HEALTH F7), by ERC project "Cello" and by ANR project MICAD.

## Notes and references

<sup>a</sup> Institut Curie, Centre National de la Recherche Scientifique, Université Pierre et Marie Curie, Unité Mixte de Recherche 168, 75005 Paris, France.

<sup>b</sup> Laboratory of Circulating Cancer Biomarker, Institut Curie, 26 rue d'Ulm, 75005 Paris, France

<sup>c</sup> Department of Medical Oncology and SIRIC, Institut Curie, 26 rue d'Ulm, 75005 Paris, France

<sup>d</sup> Université Paris Descartes, 15 rue de l'École de Médecine, 75006 Paris, France

<sup>e</sup> University of Paris-Sud, INSERM U981 "Identification of molecular predictors and new targets for cancer treatment" and Laboratory of Translational Research, Gustave Roussy, Villejuif, France.

\* To whom correspondence should be addressed:

jean-louis.viovy@curie.fr

† Current address: IBM Research GmbH, Säumerstrasse 4, 8803 Rüschlikon, Switzerland

- M.-Y. Kim, T. Oskarsson, S. Acharyya, D. X. Nguyen, X. H.-F. Zhang, L. Norton, and J. Massagué, *Cell*, 2009, **139**, 1315–26.
- F.-C. Bidard, J.-Y. Pierga, J.-C. Soria, and J. P. Thiery, *Nat. Rev. Clin. Oncol.*, 2013, **10**, 169–79.
- W. Janni, B. K. Rack, L. W. W. M. Terstappen, J.-Y. Pierga, T. Fehm, C. Hall, M. Groot, F.-C. Bidard, F. Meier-Stieger, T. Friedl, P. Fasching, and A. Lucci, in *San Antonio Breast Cancer Symposium*, 2013.
- F.-C. Bidard, D. J. Peeters, T. Fehm, F. Nolé, R. Gisbert-Criado, D. Mavroudis, S. Grisanti, D. Generali, J. A. Garcia-Saenz, J. Stebbing, C. Caldas, P. Gazzaniga, L. Manso, R. Zamarchi, A. F. de Lascoiti, L. De Mattos-Arruda, M. Ignatiadis, R. Lebofsky, S. J. van Laere, F. Meier-Stiegen, M.-T. Sandri, J. Vidal-Martinez, E. Politaki, F. Consoli, A. Bottini, E. Diaz-Rubio, J. Krell, S.-J. Dawson, C. Raimondi, A. Rutten, W. Janni, E. Munzone, V. Carañana, S. Agelaki, C. Almici, L. Dirix, E.-F. Solomayer, L. Zorzino, H. Johannes, J. S. Reis-Filho, K. Pantel, J.-Y. Pierga, and S. Michiels, *Lancet Oncol.*, 2014.

- S. T. Ligthart, F.-C. Bidard, C. Decraene, T. Bachelot, S. Delaloge, E. Brain, M. Campone, P. Viens, J.-Y. Pierga, and L. W. M. M. Terstappen, *Ann. Oncol.*, 2012, 1–8.
- S. Meng, D. Tripathy, S. Shete, R. Ashfaq, B. Haley, S. Perkins, P. Beitsch, A. Khan, D. Euhus, C. Osborne, E. Frenkel, S. Hoover, M. Leitch, E. Clifford, E. Vitetta, L. Morrison, D. Herlyn, L. W. M. M. Terstappen, T. Fleming, T. Fehm, T. Tucker, N. Lane, J. Wang, and J. Uhr, *Proc. Natl. Acad. Sci. U. S. A.*, 2004, **101**, 9393–8.
- J. den Toonder, *Lab Chip*, 2011, **11**, 375–7.
- S. Riethdorf, H. Fritsche, V. Müller, T. Rau, C. Schindlbeck, B. Rack, W. Janni, C. Coith, K. Beck, F. Jänicke, S. Jackson, T. Gornet, M. Cristofanilli, and K. Pantel, *Clin. Cancer Res.*, 2007, **13**, 920–8.
- J. Kraan, S. Sleijfer, M. H. Strijbos, M. Ignatiadis, D. Peeters, J.-Y. Pierga, F. Farace, S. Riethdorf, T. Fehm, L. Zorzino, A. G. J. Tibbe, M. Maestro, R. Gisbert-Criado, G. Denton, J. S. de Bono, C. Dive, J. A. Foekens, and J. W. Gratama, *Cytometry B. Clin. Cytom.*, 2011, **80**, 112–8.
- J. Autebert, B. Coudert, F.-C. Bidard, J.-Y. Pierga, S. Descroix, L. Malaquin, and J.-L. Viovy, *Methods*, 2012, **57**, 297–307.
- D. R. Parkinson, N. Dracopoli, B. G. Petty, C. Compton, M. Cristofanilli, A. Deisseroth, D. F. Hayes, G. Kapke, P. Kumar, J. S. Lee, M. C. Liu, R. McCormack, S. Mikulski, L. Nagahara, K. Pantel, S. Pearson-White, E. A. Punnoose, L. T. Roadcap, A. E. Schade, H. I. Scher, C. C. Sigman, and G. J. Kelloff, *J. Transl. Med.*, 2012, **10**, 138.
- I. Cima, C. Wen Yee, F. S. Iliescu, W. Min Phyo, K. Hon Lim, C. Iliescu, and M. Han Tan, *Biomicrofluidics*, 2013, **7**, 11810.
- A. a Adams, P. I. Okagbare, J. Feng, M. L. Hupert, D. Patterson, J. Göttert, R. L. McCarley, D. Nikitopoulos, M. C. Murphy, and S. a Soper, *J. Am. Chem. Soc.*, 2008, **130**, 8633–41.
- S. M. Santana, H. Liu, N. H. Bander, J. P. Gleghorn, and B. J. Kirby, *Biomed. Microdevices*, 2011.
- S. Wang, H. Wang, J. Jiao, K.-J. Chen, G. E. Owens, K. Kamei, J. Sun, D. J. Sherman, C. P. Behrenbruch, H. Wu, and H.-R. Tseng, *Angew. Chem. Int. Ed. Engl.*, 2009, **48**, 8970–3.
- S. Nagrath, L. V. Sequist, S. Maheswaran, D. W. Bell, D. Irimia, L. Ulkus, M. R. Smith, E. L. Kwak, S. Digumarthy, A. Muzikansky, P. Ryan, U. J. Balis, R. G. Tompkins, D. A. Haber, and M. Toner, *Nature*, 2007, **450**, 1235–1239.
- G. Galletti, M. S. Sung, L. T. Vahdat, M. a. Shah, S. M. Santana, G. Altavilla, B. J. Kirby, and P. Giannakakou, *Lab Chip*, 2013, **14**, 147–56.
- A. H. Talasz, A. a Powell, D. E. Huber, J. G. Berbee, K.-H. Roh, W. Yu, W. Xiao, M. M. Davis, R. F. Pease, M. N. Mindrinos, S. S. Jeffrey, and R. W. Davis, *Proc. Natl. Acad. Sci. U. S. A.*, 2009, **106**, 3970–5.
- C. Alix-Panabières and K. Pantel, *Lab Chip*, 2013.
- P. Chen, Y.-Y. Huang, K. Hoshino, and X. Zhang, *Lab Chip*, 2013, **14**, 446–58.
- A.-E. Saliba, L. Saias, E. Psychari, N. Minc, D. Simon, F.-C. Bidard, C. Mathiot, J.-Y. Pierga, V. Fraissier, J. Salamero, V. Saada, F. Farace, P. Vielh, L. Malaquin, and J.-L. Viovy, *Proc. Natl. Acad. Sci. U. S. A.*, 2010, **107**, 14524–9.
- L. Saias, J. Autebert, L. Malaquin, and J.-L. Viovy, *Lab Chip*, 2011, **11**, 822–32.
- G. M. Whitesides, E. Ostuni, S. Takayama, X. Jiang, and D. E. Ingber, *Annu. Rev. Biomed. Eng.*, 2001, **3**:335–73.

24. T. Kraus, L. Malaquin, E. Delamarche, H. Schmid, N. D. Spencer, and H. Wolf, *Adv. Mater.*, 2005, **17**, 2438–2442.
25. L. Malaquin, T. Kraus, H. Schmid, E. Delamarche, and H. Wolf, *Langmuir*, 2007, **23**, 11513–21.
26. M. Chiari, M. Cretich, and J. Horvath, *Electrophoresis*, 2000, **21**, 1521–6.
27. K. Perez-Toralla, J. Champ, M. R. Mohamadi, O. Braun, L. Malaquin, J.-L. Viovy, and S. Descroix, *Lab Chip*, 2013, **13**, 4409–18.
28. T. Kraus, L. Malaquin, H. Schmid, W. Riess, N. D. Spencer, and H. Wolf, *Nat. Nanotechnol.*, 2007, **2**, 570–6.
29. J. P. Gleghorn, E. D. Pratt, D. Denning, H. Liu, N. H. Bander, S. T. Tagawa, D. M. Nanus, P. a Giannakakou, and B. J. Kirby, *Lab Chip*, 2010, **10**, 27–9.
30. C. G. Rao, D. Chianese, G. V Doyle, M. C. Miller, T. Russell, R. A. Sanders, and L. W. M. M. Terstappen, *Int. J. Oncol.*, 2005, **27**, 49–57.
31. P. K. Vogt, M. Gymnopoulos, and J. R. Hart, *Curr. Opin. Genet. Dev.*, 2009, **19**, 12–7.
32. Y. Samuels and V. E. Velculescu, *Cell Cycle*, 2004, **3**, 1221–4.